

PROBING ELEMENTAL ABUNDANCES IN SNR 1987A USING XMM-NEWTON

KEVIN HENG^{1,2}, FRANK HABERL¹, BERND ASCHENBACH¹ & GÜNTHER HASINGER¹

Draft version October 27, 2018

ABSTRACT

We report on the latest (2007 Jan) observations of supernova remnant (SNR) 1987A from the *XMM-Newton* mission. Since the 2003 May observations of Haberl et al. (2006), 11 emission lines have experienced increases in flux by factors ~ 3 to 10 (6 ± 0.6 on average), with the 775 eV line of O VIII showing the greatest increase. Overall, we are able to make Gaussian fits to 17 emission lines in the *RGS* spectra and obtain line fluxes; we have observed 6 lines of Fe XVII and Fe XVIII previously unreported by *XMM-Newton*. A two-shock model representing plasmas in non-equilibrium ionization is fitted to the *EPIC-pn* spectra, yielding temperatures of ~ 0.4 and ~ 3 keV, as well as elemental abundances for N, O, Ne, Mg, Si, S and Fe.

We demonstrate that the abundance ratio of N and O can be constrained to $\lesssim 20\%$ accuracy ($N/O = 1.17 \pm 0.20$). Within the same confidence interval, the same analysis suggests that the C+N+O abundance varies from ~ 1.1 to 1.4×10^{-4} , verifying the *Chandra* finding by Zhekov et al. (2006) that the C+N+O abundance is lower by a factor ~ 2 compared to the value obtained in the optical/ultraviolet study by Lundqvist & Fransson (1996). Normalizing our obtained abundances by the Large Magellanic Cloud (LMC) values of Hughes, Hayashi & Koyama (1998), we find that O, Ne, Mg and Fe are under-abundant, while Si and S are over-abundant, consistent with the findings of Aschenbach (2007). Such a result has implications for both the single-star and binary accretion/merger models for the progenitor of SNR 1987A. In the context of the binary merger scenario proposed by Morris & Podsiadlowski (2006, 2007), material forming the inner, equatorial ring was expelled after the merger, implying that either our derived Fe abundance is inconsistent with typical LMC values or that iron is under-abundant at the site of Sanduleak -69°202.

Subject headings: circumstellar matter — methods: data analysis — plasmas — shock waves — supernovae: individual (SN 1987A) — ISM: supernova remnants — X-rays: individual (SN 1987A)

1. INTRODUCTION

SNR 1987A is the Rosetta Stone (Allen 1960) of Type II supernova remnants, resolved and well-studied in multiple wavebands, including the infrared (Bouchet et al. 2006; Kjaer et al. 2007), optical/ultraviolet (Grönningsson et al. 2007; Heng 2007) and radio (Gaensler et al. 2007). The physical mechanism partially powering optical/ultraviolet emission from the reverse shock is the same as the one at work in Balmer-dominated supernova remnants (Heng & McCray 2007; Heng et al. 2007). The detection of a neutrino burst confirmed the core collapse nature of the progenitor (Koshiya et al. 1987; Svoboda et al. 1987), though a pulsar has yet to be detected (Manchester 2007). A system of three rings may be the result of a binary merger between two massive stars about 20,000 years prior to the supernova explosion (Morris & Podsiadlowski 2006, 2007; hereafter MP0607). Reviews of the multi-wavelength studies of SNR 1987A can be found in McCray (1993, 2005, 2007).

Mixing of the stellar envelope and core by Rayleigh-Taylor instabilities within the progenitor star, Sanduleak -69°202, has been invoked to explain the early emergence of the 847 keV γ -ray line from SNR 1987A, which was predicted by Shibazaki & Ebisuzaki (1988) to reach its

peak around 1.1 years after the explosion, if one assumes a mixed mass of about $5M_{\odot}$ (Ebisuzaki & Shibazaki 1988). Instead, Matz et al. (1988) observed the 847 keV line ~ 6 to 8 months post-explosion, suggesting even more extensive mixing of ^{56}Co than assumed. A similar explanation (Ebisuzaki & Shibazaki 1988) was given for the early emergence of 16 to 28 keV X-rays (Sunyaev et al. 1990; Inoue et al. 1991). The γ -rays originate from the radioactive decay of ^{56}Co , while the X-rays are from the Compton degradation of the γ -rays (McCray, Shull & Sutherland 1987).

In the soft X-ray, SNR 1987A was first observed by Beuermann, Brandt & Pietsch (1994). Subsequently, Hasinger, Aschenbach & Trümper (1996) tracked a steady increase of the soft X-ray flux over 4 years with *ROSAT*. Extensive work has since been done by the *Chandra* (Michael et al. 2002; Park et al. 2002, 2004, 2005 [hereafter P05], 2006, 2007 [hereafter P07]; Zhekov et al. 2005, 2006 [hereafter Z06]) and *XMM-Newton* groups (Haberl et al. 2006, hereafter H06; Aschenbach 2007, hereafter A07). The general picture gleaned from these studies is of a bimodal plasma distribution present in the region between the forward and reverse shocks (Fig. 1). The soft X-rays (~ 0.3 to 0.5 keV) are from the decelerated shock front interacting with dense protrusions (“fingers”) on the inner, equatorial ring, while the “hard” X-rays (~ 2 to 3 keV) are from a fast shock propagating into more tenuous material. The soft X-rays appear to be correlated with optical “hot spots”, believed to

¹Max Planck Institut für extraterrestrische Physik, Giessenbachstraße, 85478 Garching, Germany

²Max Planck Institut für Astrophysik, Karl-Schwarzschild-Straße 1, 85740 Garching, Germany

be emission from the shocked fingers, appearing around the equatorial ring, while the hard X-ray and radio images exhibit structures that coincide. Between Days 6000 and 6200, the soft X-ray light curve experienced an up-turn and departure from an exponentially increasing profile, which P05 interpreted as evidence that the blast wave had reached the main body of the dense circumstellar material of the equatorial ring. Future studies on the nature of the soft X-ray light curve are relevant to the issue of pre-ionization of the supernova ejecta, which can potentially extinguish $H\alpha$ and $Ly\alpha$ emission from the reverse shock (Smith et al. 2005; Heng et al. 2006).

In the studies described, relatively little attention has been paid to the subject of inferring elemental abundances from X-ray analyses. Fits to the X-ray spectra yield N, O, Ne, Mg, S, Si and Fe abundances; such results have been tabulated and studied by Z06 and H06, using *Chandra* and *XMM*, respectively. Here, we examine such an approach using the latest *XMM* data set of SNR 1987A, taken in early 2007. In §2, we describe our observations and data reduction techniques. Our results are presented in §3. In §4, we perform a detailed error analysis of individual abundances and their ratios. We find that the N/O ratio as well as the individual N and O abundances can be constrained to $\sim 20\%$ accuracy. Our derived elemental abundances for O, Ne, Mg and Fe are under-abundant, while Si and S are over-abundant, relative to typical values for the Large Magellanic Cloud (LMC; Hughes, Hayashi & Koyama 1998). Such a result has implications for modeling the progenitor of SNR 1987A, which we discuss.

2. OBSERVATIONS & DATA REDUCTION

The latest *XMM-Newton* (Jansen, Lumb & Altieri 2001) observations of SNR 1987A were performed from 2007 Jan 17 18:23 to Jan 19 01:18 UT. For our spectral analysis, we utilize data from the CCD cameras *EPIC-pn* (Strüder et al. 2001a,b) and *EPIC-MOS* (Turner et al. 2001), and the *Reflection Grating Spectrometers (RGS)* (den Herder et al. 2001). Additional details and net exposure times for the different instruments are summarized in Table 1.

The data were processed with the *XMM-Newton Science Analysis Software (SAS)* version 7.1.0. Using `ds9`, we extracted source and background *EPIC* spectra of SNR 1987A from circular regions placed on the source and a proximate, point source-free area (Fig. 2). For the *EPIC-pn* spectra, single-pixel (PATTERN 0) events were selected; for *EPIC-MOS* all valid event patterns (PATTERN 0 to 12) were used. *RGS* spectra were produced using `rgsproc`. The spectra were binned to contain a minimum of 20 and 30 counts per bin for *EPIC* and *RGS*, respectively.

3. RESULTS

3.1. SPECTRAL FITTING

Spectral fitting was done using *XSPEC* (Arnaud 1996) version 11.3.2. We fit the reduced spectra using models with two components: a low (T_{low}) and a high (T_{high}) temperature component. Two models are considered in *XSPEC*: *VNEI+VRAYMOND* and *VPSHOCK+VPSHOCK*. In H06, the former (“Model A”) is seen to give an excellent fit (“reduced chi-square” of $\chi_r^2 \approx 1.1$) to the *EPIC-pn*

data. However, the *VRAYMOND* component of the model, which describes a plasma in ionization equilibrium, is at odds with the belief that both plasmas are in non-equilibrium ionization (NEI; Z06); we note that Park et al. (2004, 2006) found the low-temperature plasma component to be in a highly-advanced ionization state (with ionization ages $\sim 10^{12}$ to 10^{13} cm $^{-3}$ s) and can be described by a thermal plasma in collisional ionization equilibrium. The *VNEI* model is a somewhat unsatisfactory representation of the physical situation in the post-shock plasma of SNR 1987A, because it considers only one value of the ionization age/time, τ , for the entire plasma. The *VPSHOCK* model generalizes the *VNEI* one, as it integrates over portions of the plasma with different ionization ages. Borkowski, Lyerly & Reynolds (2001) showed that NEI models with a single value of τ are poor descriptions of the so-called “Sedov models” (Hamilton, Sarazin & Chevalier 1983), designed to model thermal X-ray emission from SNRs. Instead, plane-parallel models with multiple temperatures and τ are good fits to the Sedov models, further justifying the preference for the *VPSHOCK+VPSHOCK* model. We have utilized version 2.0 of the NEI models in *XSPEC*, as used by Z06; the files, with updated “inner shell processes” (Z06), were kindly provided to us by the author of the models, K. Borkowski (2007, private communication).

The data and model fits are plotted in Figs. 3 and 4. Details of the fits to the *EPIC-pn* data as well as the derived parameters are given in Table 2. For the *VPSHOCK+VPSHOCK* model, the range of ionization ages, $\tau \equiv n_e t_{\text{ion}}$, is bounded by $0 \leq \tau \leq \tau_u$. Consistent with previous studies of SNR 1987A in the X-ray, the upper limit to the ionization age, τ_u , is *higher* for the lower temperature component. The computed abundances are given relative to their *solar values* (Anders & Grevesse [1989], hereafter AG89; Wilms, Allen & McCray [2000], hereafter W00; see §4), as defined in *XSPEC*. Galactic foreground absorption is fixed at 6×10^{20} cm $^{-2}$, following H06. To account for absorption by the LMC, we take the elemental abundances to be 0.5 relative to their solar values, with the exception of helium which is kept at its solar value. To get a handle on the systematic errors, we consider both the AG89 and W00 tables. For meaningful comparisons, output abundance values must be normalized to values relative to hydrogen using the respective abundance table used. In the said version of *XSPEC*, we note that the help file for the *VPSHOCK* function erroneously lists it as being hardwired to the AG89 tables, even though it is superseded by the `abund` command (K. Arnaud 2007, private communication).

The errors are computed using the `error` function for $\Delta\chi^2 = 2.706$. In general, the dependence of the confidence level on $\Delta\chi^2$ is a non-trivial function (Wall & Jenkins 2003). Avni (1976) finds that it depends on the number of parameters that are estimated simultaneously, i.e., “interesting parameters”, and not on the total number of parameters in the fitting function. For one interesting parameter, the 90% confidence interval corresponds to $\Delta\chi^2 = 2.71$; if more interesting parameters are considered, the required value of $\Delta\chi^2$ increases. The $\Delta\chi^2 = 2.706$ level is often quoted as the “90%” confidence interval in *XSPEC* analyses of SNR 1987A — we wish to point out that this should be regarded with some

care. Following Z06 and H06, the abundances of He, C, Ar, Ca and Ni are held fixed — He and C values are taken from Lundqvist & Fransson (1996, hereafter LF96), while Ar, Ca and Ni ones are from Russell & Dopita (1992).

The VPSHOCK+VPSHOCK model is marginally superior to the VNEI+VRAYMOND one for fitting the *EPIC-pn* data — the reduced chi-square is $\chi_r^2 = 1.21$ versus 1.31. For reference, we note that the calibration spectra for *XMM* are typically fitted with a “goodness” of $\chi_r^2 \approx 1.5$. To check for consistency between the different *XMM* instruments, we have taken the VPSHOCK+VPSHOCK fit to the *EPIC-pn* data, folded it with the corresponding detector response and compared it with the *EPIC-MOS* and *RGS* spectra. All of the fit parameters are held fixed in the comparison, but the normalization is allowed to vary via a constant factor. This yields $\chi_r^2 = 1.52$ (*MOS1*), 1.41 (*MOS2*) and 1.56 (*RGS*); for the VNEI+VRAYMOND model, we get $\chi_r^2 = 1.45$, 1.46 and 1.54 instead. Full-fledged and independent fits — like for the *EPIC-pn* spectra — to the *EPIC-MOS* data and their corresponding χ_r^2 values are displayed in Fig. 4. We note that making more parameters free did not necessarily improve the fits, implying good cross calibration between the *EPIC-pn* and *EPIC-MOS* cameras.

The better counting statistics of the *EPIC-pn* data — and its wider energy coverage compared to the *RGS* — motivate us to use it as a template for obtaining the temperatures of the two plasma components. Moreover, the higher-temperature component lies beyond the energy range of the *RGS*. From performing the VPSHOCK+VPSHOCK fit to the *EPIC-pn* data, we obtain $kT_{\text{low}} = 0.4$ keV and $kT_{\text{high}} = 3.0$ keV, consistent with the values of ~ 0.5 and ~ 3 keV by Z06 (2004 Aug/Sept), who also used a two-shock, NEI model. By contrast, the VNEI+VRAYMOND fit to the *EPIC-pn* data gives $kT_{\text{low}} = 0.3$ keV and $kT_{\text{high}} = 2.4$ keV. An NEI plasma is at a higher temperature than is reflected by the ionization stages of its elements; therefore, modeling it as a plasma in collisional ionization equilibrium underestimates its temperature. We do not expect the temperatures of the plasmas to be substantially lower relative to earlier epochs, as the hot spots on the equatorial ring continue to brighten. A worthwhile future endeavor will be to obtain kT_{low} and kT_{high} for all of the existing *Chandra*, *XMM* and *Suzaku* observations of SNR 1987A, analyzed self-consistently using the same VPSHOCK+VPSHOCK model with both AG89 and W00 abundance tables.

3.2. INTEGRATED FLUX

By integrating the X-ray spectra, one can obtain fluxes in different sub-bands. Park et al. (2004) trisected the spectral range into: the 0.3 — 0.8 keV sub-band to represent the O line features (“O band”); the 0.8 — 1.2 keV sub-band for the Ne line features (“Ne band”); and the 1.2 — 8 keV sub-band for the Mg/Si lines plus any hard-tail emission features (“H band”). The soft X-ray band is commonly regarded to be in the 0.5 to 2 keV range (P05; H06), a historical convention from the era of *ROSAT* (Hasinger, Aschenbach & Trümper 1996). The “hard band” is taken to be 3 to 10 keV by P05. We integrate the *uncorrected* X-ray spectra for various sub-bands and tabulate them (for 1- σ confidence intervals) in Table 4. To correct for Galactic and LMC absorption, one sets the column densities to zero and then re-computes the fluxes.

Due to the different abundance tables used and column densities inferred, the absorption-corrected luminosities are model-dependent. Assuming a distance to the SNR 1987A of $d \approx 50$ kpc, we obtain for $L_{0.5-2\text{keV}}$: 1.95×10^{36} erg s^{-1} (VPSHOCK+VPSHOCK, W00 table), 2.32×10^{36} erg s^{-1} (VPSHOCK+VPSHOCK, AG89 table) and 2.28×10^{36} erg s^{-1} (VNEI+VRAYMOND, W00 table). For $L_{0.5-10\text{keV}}$, we get: 2.17×10^{36} erg s^{-1} (VPSHOCK+VPSHOCK, W00 table), 2.54×10^{36} erg s^{-1} (VPSHOCK+VPSHOCK, AG89 table) and 2.49×10^{36} erg s^{-1} (VNEI+VRAYMOND, W00 table). For the 2007 Jan observation of P07, $L_{0.5-10\text{keV}} \approx 2.35 \times 10^{36}$ erg s^{-1} .

3.3. LINE FITTING

For the *RGS* observations, we consider only data points between 0.45 and 1.1 keV, the range over which 11 emission lines were previously listed by H06 (see their Table 5 and also Z06). We note that 38 lines were considered by H06, but only 11 were listed so as to facilitate comparison with the *Chandra* studies. We rebin the spectra such that each bin has a minimum of 30 photon counts; we find that if the minimum count is 40, some of the lines are covered by only 2 to 3 bins. The *RGS* spectra are modeled using a thermal bremsstrahlung component for the continuum and a set of Gaussian profiles for the lines. We first fit only to the 11 lines of N VII, O VII, O VIII, Ne IX and Ne X (Fig. 5). We see that several lines are not fitted by such a model — we propose that 6 additional lines are now observed: the 725, 727, 739, 812 and 826 eV lines of Fe XVII; and possibly the 873 eV line of Fe XVIII. (See Table 1 of Behar et al. [2001] and Fig. 2 of Rasmussen et al. [2001] for details on the expected lines in SNR spectra within the *RGS* energy range.) The detection of the iron lines lends support to our derived Fe abundance and its implications (see §4).

Following H06, we force the widths of all of the lines to be the same. The more energetic lines are probably powered by the faster shocks, and should therefore have larger widths. A more realistic approach is therefore to model the widths as some increasing function of the ionization potential of each line. However, the rather narrow energy range considered here does not warrant such an approach. The redshift inferred from the fits is $(1.88 \pm 0.26) \times 10^{-3}$. The Gaussian width of the lines is $\sigma_{\text{fit}} = 0.87 \pm 0.11$ eV — the full width at half-maximum (FWHM) value is 2.05 ± 0.26 eV, which is narrower than the 5.3 ± 1.0 eV value of H06. The measured Gaussian width is indicative of the velocities of the shocks responsible for the X-ray emission — the velocities inferred are $v_s \sim 0.87c/E_{\text{eV}}$, where E_{eV} is the energy of a given line in electron volts. For a 1 keV line, we have $v_s \sim 300$ km s^{-1} , consistent with the *Chandra* studies of Z06, who find that the X-ray emission originate from shocks with $300 \lesssim v_s \lesssim 1700$ km s^{-1} .

The fluxes we obtain from fitting to these lines are given in Table 5. In Fig. 6, we show the relative increases in flux of the lines (or line complexes) measured in our study versus those of H06. Since 2003 May, the line fluxes have increased by factors ~ 3 to 10 — the 775 eV line of O VIII shows the strongest increase. On average, the lines show an increase of 6.0 ± 0.6 over ~ 4 years. The 2003 May soft X-ray flux was measured by H06 to be $F_{0.5-2\text{keV}} = (8.10 \pm 0.09) \times 10^{-13}$ erg cm^{-2} s^{-1} . Our

2007 Jan value is $F_{0.5-2\text{keV}} = (3.34 \pm 0.04) \times 10^{-12}$ erg $\text{cm}^{-2} \text{s}^{-1}$, corresponding to an increase of 4.1 ± 0.1 in the soft X-ray flux. Generally, the same shocks that are responsible for the brightening of the optical and soft X-ray hot spots are also powering the lines. The differences in the flux increases may be an indication that the equivalent widths of the lines are changing, which is evidence for the evolution of the elemental abundances. Such an investigation is deferred to future studies, when one can obtain smaller error bars for the relative increases of the line fluxes (Fig. 6).

4. DISCUSSION

4.1. INDIVIDUAL ABUNDANCES & THEIR RATIOS

We compare the derived elemental abundances to those of Z06 and H06 and list them *relative to hydrogen* in Table 3; uncertainties in the AG89 and W00 abundance tables are not propagated. We emphasize that care must be taken to specify the abundance table used, as this may lead to widely differing values of the derived abundances (relative to hydrogen). In modeling the LMC absorption, Z06 used the elemental abundance table of AG89, while H06 chose the table of W00 because the lower oxygen abundance fitted the K absorption edge in the *EPIC* data better.

Fransson et al. (1989) found $\text{N/O} = 1.6 \pm 0.8$, about 12 times higher³ than the AG89 solar value, which they interpret as evidence of substantial CNO processing. LF96 found $\text{N/O} = 1.1 \pm 0.4$, while Sonneborn et al. (1997) found $\text{N/O} = 1.7 \pm 0.5$. All three of these values were derived from optical/ultraviolet data. Next, we turn our attention to the N/O ratio derived from X-ray studies. Linearly propagating the errors listed by Z06, we find that their results yield $\text{N/O} = 1.10^{+0.47}_{-0.45}$; they remark that their derived C, N and O abundance, $\text{C+N+O} \approx 1.98 \times 10^{-4}$, is lower by about a factor of 2 compared to the 3.72×10^{-4} value of LF96. Model A (VNEI+VRAYMOND) in H06 yields $\text{C+N+O} \approx 1.67 \times 10^{-4}$ and a rather wide range in the nitrogen-to-oxygen ratio, $\text{N/O} = 1.33^{+1.47}_{-0.71}$. Our VPSHOCK+VPSHOCK fit to the *EPIC-pn* data yields $\text{C+N+O} \approx 1.29 \times 10^{-4}$ and $\text{N/O} = 1.17^{+0.37}_{-0.34}$ (using the W00 table); we call this combination of N and O the “best fit point”. Note that the C abundance is held fixed at 0.09 relative to solar ($\sim 3 \times 10^{-5}$ relative to hydrogen) for the C+N+O values derived from the X-ray studies.

We next perform a more careful analysis of the N/O ratio. We first generate a χ^2 map quantifying the interdependence of the fits to the N and O abundance. Contour lines in the χ^2 map form “error ellipses”, which are shown for different $\Delta\chi^2$ values from the best fit point (Fig. 7). At the $\Delta\chi^2 = 2.706$ level, $\text{N/O} = 1.17 \pm 0.20$ for the *EPIC-pn* data. In linearly propagating the errors in the individual abundances, one is in essence adopting the largest possible range of ratios, which can be visualized as the edges of a rectangle in the contour map. Our error analysis improves the uncertainties because it considers only values of the abundance ratio within the specified contour. Within the same confidence interval considered, the corresponding C+N+O value is from ~ 1.1 to 1.4×10^{-4} . We see that the errors in the N/O

ratio and the individual N and O abundances can be constrained at the $\sim 20\%$ level. We thus confirm the C+N+O under-abundance noted by the *Chandra* studies of Z06, who suggest a couple of physical reasons for such a result: the sub-LMC abundance of C+N+O within the progenitor star, Sanduleak -69°202, and/or an extra source of possibly non-thermal, X-ray continuum.

We perform the same analysis for N/S (Fig. 8). Again using the W00 table, linear propagation of the errors in the abundances obtained from the VPSHOCK+VPSHOCK fit yields $\text{N/S} = 4.59^{+1.51}_{-1.36}$, while the error ellipse analysis gives $\text{N/S} = 4.59^{+1.59}_{-1.33}$. The iron, nitrogen and oxygen lines are predominantly from the lower energy part ($\lesssim 1$ keV) of the spectrum, while the sulphur lines are situated between ~ 2.2 and 3.1 keV. (The silicon lines are located between ~ 1.8 and 2.2 keV.) Abundance ratios based on lines of widely differing energies lead to rounder error ellipses — “error circles”. In such cases, a more thorough error analysis will not constrain the abundance ratio better, as in the case of N/S. This is partially an instrumental effect — when the energy resolution is comparable to the spacing of the lines, the line complexes overlap and are only partially resolved. There is also the issue of choosing a coordinate system in which the fitting parameters are “orthogonal”. Hydrogen and helium have no X-ray lines — their abundances are derived from the strength of the X-ray continuum. When the pair of elements considered are situated close to each other in energy, the hydrogen abundance has to first order a linear dependence on the continuum strength. Thus, the ratio of the considered abundances is tightly constrained as the individual abundances track each other closely. By contrast, when the pair of abundances considered are located far apart in energy, this linear dependence of hydrogen abundance on the continuum is broken as the dominant uncertainties are in temperature rather than in flux. Orthogonality is now absent. To attain orthogonality for such pairs of lines, one has to construct models that directly fit to the abundance ratio considered, an approach which is not explored in this paper.

The error in the abundance ratios increases as one moves a given $\Delta\chi^2$ away from the minimum point. In Fig. 9, we compute the mean error sustained by the various ratios as a function of $\Delta\chi^2$. According to Avni (1976), if three interesting parameters are considered (see §3.1), the 90% confidence interval is situated at $\Delta\chi^2 = 6.25$. In this case, the N/O abundance ratio suffers from errors $\sim 25\%$.

4.2. THE PROGENITOR OF SNR 1987A: SINGLE-STAR OR BINARY MODEL?

A more revealing approach to analyze the elemental abundances is to normalize the results listed in Table 3 by the “canonical” values of the LMC abundances (Hughes, Hayashi & Koyama 1998). These were derived using a sample of 7 middle-aged SNRs in the LMC (N23, N49, N63A, DEM 71, N132D, 0453-68.5 and N49B). This approach was first explored by A07, who showed that the normalized abundances appear to cluster in two groups: N, O, Ne, Mg and Fe are slightly more than half their LMC values, while Si, S and Ni exceed their LMC values.

We generalize the A07 approach by considering both sets of abundances derived from using the AG89 and W00

³ The AG89 and W00 values for solar nitrogen-to-oxygen abundance are $\text{N/O} = 0.132$ and 0.110 by number, respectively.

tables. The normalized abundance, relative to its respective LMC value, is $R_{87A/LMC}$; it is plotted as a function of the elemental mass number in Fig. 10. The error bars for $R_{87A/LMC}$ are computed by linearly propagating the errors listed in Table 3 and in Hughes, Hayashi & Koyama (1998). We caution that additional systematic errors may be present that are not taken into account. For example, the derived abundance for Fe is a sensitive function of temperature and may vary substantially when small changes are made to T_{low} ⁴.

We see that the elements O, Ne, Mg and Fe are under-abundant, while Si and S are over-abundant, consistent with the findings of A07. With the exception of Fe, there is a tendency for $R_{87A/LMC}$ to increase with larger elemental mass number, a trend that is independent of the AG89 or W00 tables, though we note that it is more pronounced with the latter. The Fe abundance derived is essentially independent of the AG89 or W00 tables, and is under-abundant by about 70% relative to the LMC⁵. The under-abundance of Fe and O was previously noted by Hasinger et al. (2006), who argued for the existence of iron-oxygen “rust grains”. The reduced abundance of Fe alone suggests that the iron is locked up in dust grains. However, Dwek & Arendt (2007) showed from an analysis of the infrared-to-X-ray flux ratio — $\mathcal{R}_{IRX} < 1$ versus the theoretically expected value of $\sim 10^2$ to 10^3 — that the dust in SNR 1987A is severely depleted compared to standard dust-to-gas mass ratios in the LMC, suggesting low dust condensation efficiency or dust destruction in the hot X-ray gas. In fact, \mathcal{R}_{IRX} was shown to *decrease* with time, which is direct evidence for dust destruction. Our derived plasma temperatures are consistent with this scenario — even if dust could form, it would be destroyed at these temperatures.

In light of Fig. 10, the central question to ask is whether the progenitor of SNR 1987A arose from a single star or a binary system? Sanduleak -69°202 was known to be a blue supergiant (BSG) at the time of the supernova explosion, contrary to the expectation that massive stars end their lives as red supergiants (RSGs). Observations of low-velocity, nitrogen-rich circumstellar material are interpreted as the progenitor star being a RSG until about $\sim 20,000$ years before its death (Fransson et al. 1989). Such a time scale has in turn been interpreted as the Kelvin-Helmholtz time of the helium core (Woosley et al. 1997). This BSG-RSG-BSG evolution remains one of the greatest challenges for the single-star model (Woosley et al. 1997; Woosley, Heger & Weaver 2002), as is the observed system of three rings produced $\sim 20,000$ years before the explosion. The favored single-star models require a combination of reduced metallicity and “restricted semi-convection” (Woosley 1988), the former of which is supported by our derived abundance ratios. An additional challenge for the single-star model is to reproduce the over-abundance of Si and S (Fig. 10), which may require the invoking of some non-standard mixing process (H.-T. Janka 2007, private communication).

Binary solutions to Sanduleak -69°202 are sub-divided into accretion and merger models (see Woosley, Heger &

Weaver [2002] and references therein). The binary accretion models allow helium- and nitrogen-rich material to be added to the progenitor star and require the disappearance of the mass donor in an earlier supernova event. In the binary merger scenario proposed by MP0607, two stars with masses $\sim 5M_{\odot}$ and $\sim 15M_{\odot}$ are initially orbiting each other with a period ~ 10 years. The more massive companion transfers mass to the less massive star only after the former has completed helium burning in the core. A common envelope (Paczynski 1976) is formed, during which core material from the primary star is dredged up to the surface. The merger process takes a few hundred years, culminating in an initially over-sized RSG, which loses its excess thermal energy over a few thousand years to become a BSG. The spun-up, rapidly rotating BSG produces a fast stellar wind, sweeping up ejecta associated with the merger, producing the triple ring nebula we now see in projection. The nearly axisymmetric but highly non-spherical nature of the rings suggests that rotation played a role in their formation and is consistent with the proposed scenario. The beauty of the model lies in the fact that it requires no physically ad hoc assumptions — apart from a small kick of $\sim 2 \text{ km s}^{-1}$ given to the ejecta to displace the center of the outer rings from their symmetry axis — and makes a number of predictions. In their favored model, MP0607 assert that the outer rings are ejected before the stellar core material is dredged up, while the inner, equatorial ring — the site of the observed X-ray emission — is ejected *afterwards*⁶. A relevant consequence of this model is that the dredged-up heavy elements will manifest themselves in the form of X-ray emission lines. This may explain the trend we see in Fig. 10 — the challenge for binary merger models is to reproduce the derived $R_{87A/LMC}$ values.

Stellar nucleosynthesis can add and *not* subtract iron — in the context of the MP0607 binary merger model, we expect $R_{87A/LMC}(\text{Fe}) \geq 1$. We are again led to the question: where is the iron? If the Fe abundance derived is an upper limit on the iron used to form Sanduleak -69°202, then it is clearly inconsistent with “standard” Fe abundances in the LMC. An alternative interpretation is that there is a strong spatial variation in the Fe abundance throughout the LMC, such that the iron is sub-LMC at the site of SN 1987A and equal to its LMC abundance elsewhere. The C+N+O under-abundance suggested in §4.1 supports such a conclusion. An improvement over using the Hughes, Hayashi & Koyama (1998) *ASCA* abundance values is to re-analyze and expand upon their SNR sample using *Chandra* and *XMM*. Existing studies (e.g., Hughes et al. 2006) tend to pick out regions of interest that may include ejecta enrichment; instead, X-ray emission should be extracted from the *entire* blast wave, from which average abundances can be inferred. Future studies will be invaluable towards resolving these issues.

K.H. acknowledges the kind hospitality and financial support of: the Max Planck Institutes for Astrophysics (MPA) and Extraterrestrial Physics (MPE) during June to October 2007, where he was a visiting postdoctoral scientist; and the Lorentz Center (Leiden) during the August 2007 workshop, “From Massive Stars to Supernova Rem-

⁴ The Fe abundance obtained from the *VPSHOCK+VPSHOCK* fit (W00 table) varies by $\sim 16\%$ when T_{low} is changed by $\sim 10\%$.

⁵ The O abundance relative to H for the AG89 and W00 tables are the same.

⁶ As noted by MP0607, this hypothesis is verifiable/refutable, as the inner ring should exhibit helium enhancement and more CNO processing relative to the outer rings.

FIG. 1.— Schematic representation of the physical configuration in SNR 1987A. Courtesy of Richard McCray (JILA, University of Colorado) and the *Chandra* press release team. *Figure has been omitted due to large file size; please refer to the electronic version of the Astrophysical Journal for this figure.*

nants”. He thanks Dick McCray, Sangwook Park, Svet Zhekov, Jack Hughes, John Raymond, Philipp Podsiadlowski, Rashid Sunyaev, Peter Lundqvist, Claes Fransson, Dmitrijs Docenko, Thomas Janka, Carlos Badenes, Roger Chevalier, Nathan Smith and Jacco Vink for engaging and helpful discussions. Special mentions go out to: Dick and John, who provided a crash course on non-equilibrium ionization plasmas during a sunny bicycle ride in Leiden; Svet, who pointed out relevant

material on X-ray physics, as well as for critical comments following his meticulous scrutiny of the manuscript. The authors are collectively grateful to Kazik Borkowski for providing the updated VPSHOCK model files for use in XSPEC. The *XMM-Newton* project is supported by the *Bundesministerium für Wirtschaft und Technologie/Deutsches Zentrum für Luft- und Raumfahrt* (BMWi/DLR, FKZ 50 OX 001) and the Max Planck Society.

REFERENCES

- Allen, D.C. 1960, *Proceedings of the American Philosophical Society (PAPhS)*, 104, 5
- Arnaud, K.A. 1996, in *Astronomical Data Analysis Software and Systems V*, ASP Conference Series, 101, 17
- Aschenbach, B. 2007, *Supernova 1987A: Twenty Years After: Supernovae and Gamma-Ray Bursters*, eds. S. Immler, K. W. Weiler and R. McCray, American Institute of Physics, New York (arXiv:0705.3406) [A07]
- Anders, E., & Grevesse, N. 1989, *Geochim. Cosmochim. Acta*, 53, 197 [AG89]
- Avni, Y. 1976, *ApJ*, 210, 642
- Behar, E., Rasmussen, A.P., Griffiths, R.G., Dennerl, K., Audard, M., Aschenbach, B., & Brinkman, A.C. 2001, *A&A*, 365, L242
- Beuermann, K., Brandt, S., & Pietsch, W. 1994, *A&A*, 281, L45
- Bouchet, P., et al. 2006, *ApJ*, 650, 212
- Borkowski, K.J., Lyerly, W.J., & Reynolds, W.P. 2001, *ApJ*, 548, 820
- Dwek, E., & Arendt, R.G. 2007, *Supernova 1987A: Twenty Years After: Supernovae and Gamma-Ray Bursters*, eds. S. Immler, K. W. Weiler and R. McCray, American Institute of Physics, New York (arXiv:0705:3796)
- Ebisuzaki, T., & Shibazaki, N. 1988, *ApJL*, 327, L5
- Fransson, C., Cassatella, C., Gilmozzi, R., Kirshner, R.P., Panagia, N., Sonneborn, G., & Wamsteker, W. 1989, *ApJ*, 336, 429
- Gaensler, B.M., Staveley-Smith, L., Manchester, R.N., Kesteven, M.J., Ball, L., & Tzioumis, A.K. 2007, *Supernova 1987A: Twenty Years After: Supernovae and Gamma-Ray Bursters*, eds. S. Immler, K. W. Weiler and R. McCray, American Institute of Physics, New York (arXiv:0705.0057)
- Gröningsson, P., et al. 2007, *A&A*, in press (astro-ph/0703788)
- Haberl, F., Geppert, U., Aschenbach, B., & Hasinger, G. 2006, *A&A*, 460, 811 [H06]
- Hamilton, A.J.S., Sarazin, C.L., & Chevalier, R.A. 1983, *ApJS*, 51, 115
- Hasinger, G., Aschenbach, B., & Trümper, J. 1996, *A&A*, 312, L9
- Hasinger, G., et al. 2006, 36th COSPAR Scientific Assembly, meeting abstract #3016
- Heng, K., et al. 2006, *ApJ*, 644, 959
- Heng, K., & McCray, R. 2007, *ApJ*, 654, 923
- Heng, K. 2007, *Supernova 1987A: Twenty Years After: Supernovae and Gamma-Ray Bursters*, eds. S. Immler, K. W. Weiler and R. McCray, American Institute of Physics, New York (arXiv:0704.1304)
- Heng, K., van Adelsberg, M., McCray, R., & Raymond, J.C. 2007, *ApJ*, 668, 275
- Hughes, J.P., Hayashi, I., & Koyama, K. 1998, *ApJ*, 505, 732
- Hughes, J.P., Rafelski, M., Warren, J.S., Rakowski, C., Slane, P., Burrows, D., & Nousek, J. 2006, *ApJ*, 645, L117
- Inoue, H., et al. 1991, *Publ. Astron. Soc. Jpn.*, 43, 213
- Jansen, F., Lumb, D., & Altieri, B., et al. 2001, *A&A*, 365, L1
- Kjaer, K., Leibundgut, B., Fransson, C., Gröningsson, P., Spyromilio, J., & Kissler-Patig, M. 2007, *A&A*, 471, 617
- Koshiha, M., et al. 1987, *IAU Circ.*, 4338, 1
- Nishimura, J. 1988, *A&A*, 197, L7
- Lundqvist, P., & Fransson, C. 1996, *ApJ*, 464, 924
- Manchester, R.N. 2007, *Supernova 1987A: Twenty Years After: Supernovae and Gamma-Ray Bursters*, eds. S. Immler, K. W. Weiler and R. McCray, American Institute of Physics, New York (arXiv:0708.2372)
- Matz, S.M., Share, G.H., Leising, M.D., Chupp, E.L., Vestrand, W.T., Purcell, W.R., Strickman, M.S., & Reppin, C. 1988, *Nature*, 331, 4
- McCray, R., Shull, J.M., & Sutherland, P. 1987, *ApJL*, 317, L73
- McCray, R. 1993, *ARAA*, 31, 175
- McCray, R. 2005, in *IAU Colloq. 192, Cosmic Explosions*, eds. J.M. Marcaide & K.W. Weiler (Heidelberg: Springer), 77
- McCray, R. 2007, *Supernova 1987A: Twenty Years After: Supernovae and Gamma-Ray Bursters*, eds. S. Immler, K. W. Weiler and R. McCray, American Institute of Physics, New York
- Michael, E., et al. 2002, *ApJ*, 574, 166
- Morris, T., Podsiadlowski, P. 2006, *MNRAS*, 365, 2 [MP0607]
- Morris, T., Podsiadlowski, P. 2007, *Science*, 315, 5815 [MP0607]
- Paczynski, B. 1976, pg. 75, in *Structure and Evolution of Close Binary Systems*, eds. P. Eggleton, S. Mitton and J. Whelan, Reidel Publishing Co., Dordrecht
- Park, S., Burrows, D.N., Garmire, G.P., Nousek, J.A., McCray, R., Michael, E., & Zhekov, S.A. 2002, *ApJ*, 567, 314
- Park, S., Zhekov, S.A., Burrows, D.N., Garmire, G.P., & McCray, R. 2004, *ApJ*, 610, 275
- Park, S., Zhekov, S.A., Burrows, D.N., & McCray, R. 2005, *A pJ*, 634, L73 [P05]
- Park, S., Zhekov, S.A., Burrows, D.N., Garmire, G.P., Racusin, J.L., & McCray, R. 2006, *ApJ*, 646, 1001
- Park, S., Burrows, D.N., Garmire, G.P., McCray, R., Racusin, J.L., & Zhekov, S.A. 2007, *Supernova 1987A: Twenty Years After: Supernovae and Gamma-Ray Bursters*, eds. S. Immler, K. W. Weiler and R. McCray, American Institute of Physics, New York (arXiv:0704.0209) [P07]
- Rasmussen, A.P., Behar, E., Kahn, S.M., den Herder, J.W., & van der Heyden, K. 2001, *A&A*, 365, L231
- Russell, S.C., & Dopita, M.A. 1992, *ApJ*, 384, 508
- Shibazaki, N., Ebisuzaki, T. 1988, *ApJL*, 327, L9
- Smith, N., Zhekov, S.A., Heng, K., McCray, R., Morse, J.A., & Gladders, M. 2005, *ApJ*, 635, L41
- Sonneborn, G., Fransson, C., Lundqvist, P., Cassatella, A., Gilmozzi, R., Kirshner, R.P., Panagia, N., & Wamsteker, W. 1997, *ApJ*, 477, 848
- Strüder, L., et al. 2001, *A&A*, 365, L18
- Strüder, L., et al. 2001, *A&A*, 375, L5
- Sunyaev, R.A., et al. 1990, *Sov. Astron. Lett.*, 16, 3
- Svoboda, R., et al. 1987, *IAU Circ.*, 4340, 1
- Turner, M.J.L., et al. 2001, *A&A*, 365, L27
- den Herder, J.W., et al. 2001, *A&A*, 365, L7
- Wall, J.V., & Jenkins, C.R. 2003, *Practical Statistics for Astronomers* (UK: Cambridge University Press)
- Wilms, J., Allen, A., & McCray, R. 2000, *ApJ*, 542, 914
- Woolley, S.E. 1988, *ApJ*, 330, 218
- Woolley, S.E., Heger, A., Weaver, T.A., & Langer, N. 1997 (astro-ph/9705146)
- Woolley, S.E., Heger, A., & Weaver, T.A. 2002, *Reviews of Modern Physics*, 74, 1015
- Zhekov, S.A., McCray, R., Borkowski, K.J., Burrows, D.N., & Park, S. 2005, *ApJ*, 628, L127
- Zhekov, S.A., McCray, R., Borkowski, K.J., Burrows, D.N., & Park, S. 2006, *ApJ*, 645, 293 [Z06]

TABLE 1
XMM-Newton OBSERVATIONS OF SNR 1987A

Instrument	Read-out Mode	Filter	Satellite Revolution	Date	Time (UT)	Net Exposure (s)
<i>EPIC-pn</i>	FF, 73 ms	Medium	1302	2007 Jan 17—19	19:28—01:18	93723
<i>EPIC-MOS1</i>	FF, 2.6 s	Medium	1302	2007 Jan 17—19	18:24—01:18	109479
<i>EPIC-MOS2</i>	FF, 2.6 s	Medium	1302	2007 Jan 17—19	18:24—01:18	109560
<i>RGS1</i>	Spectro	—	1302	2007 Jan 17—19	18:23—01:19	110528
<i>RGS2</i>	Spectro	—	1302	2007 Jan 17—19	18:23—01:19	110475

TABLE 2
COMPARISON OF THE VNEI+VRAYMOND AND THE VPSHOCK+VPSHOCK MODELS

Parameter	VNEI+VRAYMOND	VPSHOCK+VPSHOCK	VPSHOCK+VPSHOCK
	W00♣	AG89◇	W00♣
χ^2	820.2032	805.6812	755.9608
$N_{\text{dof}}^{\clubsuit}$	624	623	623
χ_r^2	1.314428	1.293228	1.213420
$kT_{\text{low}}^{\ddagger}$ (keV)	$0.320^{+0.010}_{-0.009}$	$0.419^{+0.016}_{-0.020}$	$0.434^{+0.018}_{-0.008}$
$kT_{\text{high}}^{\ddagger}$ (keV)	$2.42^{+0.175}_{-0.176}$	$2.88^{+0.21}_{-0.15}$	$2.99^{+0.24}_{-0.22}$
Galactic N_{H} (10^{21} cm^{-2}) [†]	0.6	0.6	0.6
LMC N_{H} (10^{21} cm^{-2})	3.13 ± 0.14	2.37 ± 0.10	$2.56^{+0.07}_{-0.11}$
$\tau_u(T_{\text{low}})$ ($10^{11} \text{ cm}^{-3} \text{ s}$)	—	$8.63^{+1.60}_{-0.98}$	$8.33^{+1.02}_{-1.20}$
$\tau_u(T_{\text{high}})$ ($10^{11} \text{ cm}^{-3} \text{ s}$)	$1.19^{+0.31\heartsuit}_{-0.24}$	$2.46^{+0.79}_{-0.31}$	$2.21^{+1.44}_{-0.75}$
He [†]	2.57	2.57	2.57
C [†]	0.09	0.09	0.09
N	$0.116^{+0.172}_{-0.106}$	0.303 ± 0.060	$0.536^{+0.108}_{-0.091}$
O	$0.0228^{+0.0074}_{-0.0058}$	$0.0475^{+0.0045}_{-0.0044}$	$0.0502^{+0.0058}_{-0.0060}$
Ne	$0.157^{+0.017}_{-0.015}$	$0.156^{+0.012}_{-0.007}$	$0.204^{+0.017}_{-0.018}$
Mg	$0.208^{+0.021}_{-0.019}$	$0.116^{+0.007}_{-0.008}$	$0.168^{+0.011}_{-0.015}$
Si	$0.743^{+0.068}_{-0.064}$	$0.262^{+0.025}_{-0.017}$	$0.479^{+0.046}_{-0.030}$
S	$0.689^{+0.119}_{-0.111}$	$0.452^{+0.059}_{-0.077}$	$0.585^{+0.075}_{-0.074}$
Ar [†]	0.54	0.54	0.54
Ca [†]	0.34	0.34	0.34
Fe	$0.0397^{+0.0038}_{-0.0033}$	$0.0630^{+0.0041}_{-0.0018}$	$0.0895^{+0.0050}_{-0.0060}$
Ni [†]	0.62	0.62	0.62

Note: Abundances of elements are listed relative to solar.

† Parameter is held fixed (see text).

‡ In the VNEI+VRAYMOND model, the low and high temperature components are from the VRAYMOND and VNEI fits, respectively.

♣ Number of degrees of freedom in fit.

◇ Abundance table in XSPEC from Anders & Grevesse (1989).

♠ Abundance table in XSPEC from Wilms, Allen & McCray (2000).

♥ VNEI model considers only one value of $\tau = \tau_u$.

FIG. 2.— XMM-Newton EPIC image of the region around SNR 1987A. The red-green-blue (RGB) color image is composed of images from three energy bands (0.2—1.0, 1.0—2.0 and 2.0—4.5 keV) and from all three of the EPIC instruments (*PN*, *MOS1* and *MOS2*). The individual images are exposure-corrected and out-of-time event-subtracted (for *EPIC-pn*). The source and background extraction regions used for the spectral analysis are denoted by “1987A” and “bg”, respectively. The blue, arc-like structures are due to photons from the bright X-ray binary LMC X-1 (located outside the field-of-view), which are singly-reflected on the mirror shells. *Figure has been omitted due to large file size; please refer to the electronic version of the Astrophysical Journal for this figure.*

TABLE 3
ELEMENTAL ABUNDANCES FROM DIFFERENT STUDIES (RELATIVE TO HYDROGEN)

Element	Z06 \diamond	H06 \clubsuit	This Study \diamond	This Study \clubsuit
	VPSHOCK+VPSHOCK	VNEI+VRAYMOND	VPSHOCK+VPSHOCK	VPSHOCK+VPSHOCK
N	$(8.64^{+2.58}_{-1.91})_{-5}$	$(7.47^{+4.85}_{-2.52})_{-5}$	$(3.40 \pm 0.67)_{-5}$	$(5.00^{+1.01}_{-0.85})_{-5}$
O	$(7.83^{+1.02}_{-1.48})_{-5}$	$(5.62^{+2.55}_{-1.11})_{-5}$	$(4.04^{+0.38}_{-0.37})_{-5}$	$(4.27^{+0.49}_{-0.51})_{-5}$
Ne	$(3.57^{+0.62}_{-0.49})_{-5}$	$(2.95^{+0.86}_{-0.49})_{-5}$	$(1.92^{+0.15}_{-0.09})_{-5}$	$(2.51^{+0.21}_{-0.22})_{-5}$
Mg	$(9.12 \pm 1.52)_{-6}$	$(1.05^{+0.31}_{-0.23})_{-5}$	$(4.41^{+0.27}_{-0.30})_{-6}$	$(6.54^{+0.43}_{-0.58})_{-6}$
Si	$(9.93^{+1.42}_{-2.13})_{-6}$	$(2.34^{+0.57}_{-0.43})_{-5}$	$(9.30^{+0.89}_{-0.60})_{-6}$	$(1.70^{+0.16}_{-0.11})_{-5}$
S	$(7.30^{+2.43}_{-2.11})_{-6}$	$(5.96^{+3.72}_{-3.35})_{-6}$	$(7.33^{+0.96}_{-1.25})_{-6}$	$(1.09 \pm 0.14)_{-5}$
Fe	$(7.48^{+0.47}_{-0.94})_{-6}$	$(1.33^{+0.41}_{-0.28})_{-6}$	$(2.95^{+0.19}_{-0.08})_{-6}$	$(2.83^{+0.16}_{-0.19})_{-6}$

Note: A_b is shorthand notation for $A \times 10^b$.

\diamond Abundance table in XSPEC from Anders & Grevesse (1989).

\clubsuit Abundance table in XSPEC from Wilms, Allen & McCray (2000).

TABLE 4
ABSORPTION-UNCORRECTED *EPIC-pn* FLUXES IN VARIOUS SUB-BANDS

Sub-band	photons $\text{cm}^{-2} \text{s}^{-1}$	erg $\text{cm}^{-2} \text{s}^{-1}$
0.2 — 0.8 keV	$(1.16 \pm 0.01)_{-3}$	$(1.14 \pm 0.01)_{-12}$
0.8 — 1.2 keV	$(1.01^{+0.02}_{-0.01})_{-3}$	$(1.54^{+0.03}_{-0.06})_{-12}$
1.2 — 8 keV	$(4.93^{+0.11}_{-0.15})_{-4}$	$(1.53^{+0.04}_{-0.05})_{-12}$
0.5 — 2 keV	$(2.28 \pm 0.02)_{-3}$	$(3.34 \pm 0.04)_{-12}$
3 — 10 keV	$(5.31^{+0.16}_{-0.34})_{-5}$	$(3.83^{+0.11}_{-0.23})_{-13}$
0.5 — 10 keV	$(2.42^{+0.02}_{-0.03})_{-3}$	$(4.05 \pm 0.07)_{-12}$
0.2 — 10 keV	$(2.67^{+0.03}_{-0.02})_{-3}$	$(4.24^{+0.06}_{-0.05})_{-12}$

Note: $1\text{-}\sigma$ (68%) confidence intervals; A_b is shorthand notation for $A \times 10^b$.

TABLE 5
LINE FLUXES FROM *RGS* OBSERVATIONS

Line	Energy (eV)	Flux (10^{-5} photons $\text{cm}^{-2} \text{s}^{-1}$)
N VII	500	$18.67^{+1.45}_{-1.42}$
O VII	561	$4.94^{+1.19}_{-1.73}$
O VII	569	$1.05^{+2.12}_{-1.05}$
O VII	574	$8.92^{+1.14}_{-2.37}$
O VIII	654	$25.18^{+2.13}_{-1.14}$
O VII	666	$3.21^{+0.65}_{-1.37}$
Fe XVII	725	$3.83^{+0.74}_{-1.83}$
Fe XVII	727	$12.98^{+1.17}_{-2.05}$
Fe XVII	739	$7.12^{+0.63}_{-1.46}$
O VIII	775	$9.40^{+0.84}_{-1.12}$
Fe XVII	812	$5.70^{+2.31}_{-0.47}$
Fe XVII	826	$16.00^{+2.43}_{-0.61}$
Fe XVIII	873	$6.00^{+0.77}_{-1.10}$
Ne IX	905	$8.96^{+1.16}_{-1.63}$
Ne IX	915	$1.81^{+2.58}_{-0.82}$
Ne IX	922	$18.87^{+1.17}_{-2.86}$
Ne X	1022	$17.75^{+1.35}_{-2.37}$
O VII	561+569+574	$14.91^{+4.45}_{-5.15}$
Ne IX	905+915+922	$29.64^{+4.91}_{-5.31}$

Note: $\Delta\chi^2 = 2.706$ confidence intervals.

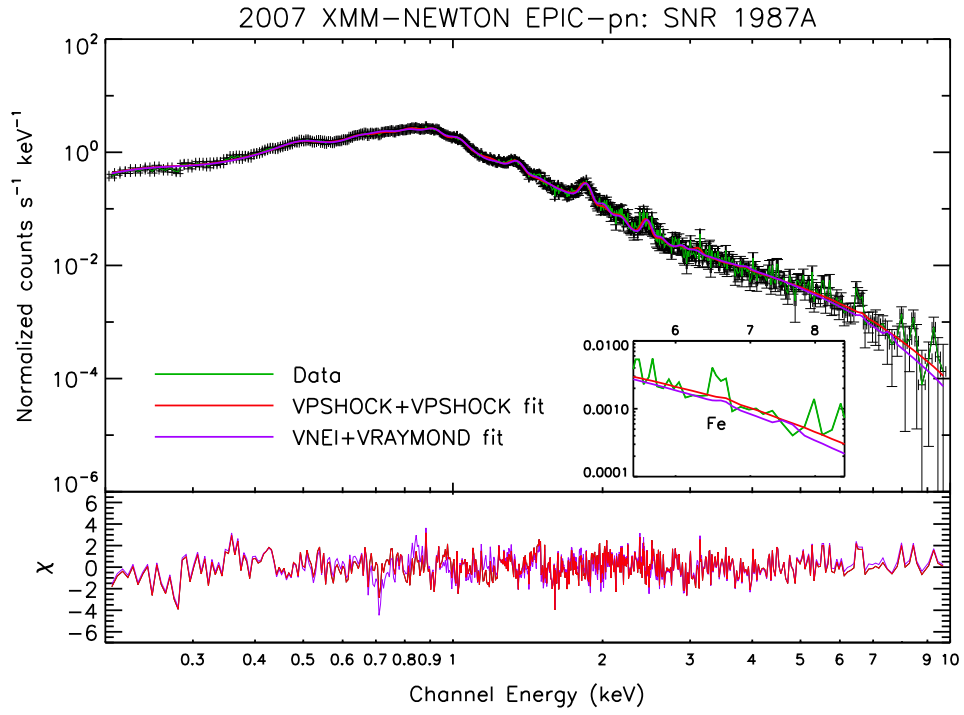


FIG. 3.— *XMM EPIC-pn* data, fitted by the VNEI+VRAYMOND and VPSHOCK+VPSHOCK models in XSPEC. The insert zooms in on a possible detection of the Fe $K\alpha$ line. Details of the model fits, as well as the derived parameter values, are given in Table 2.

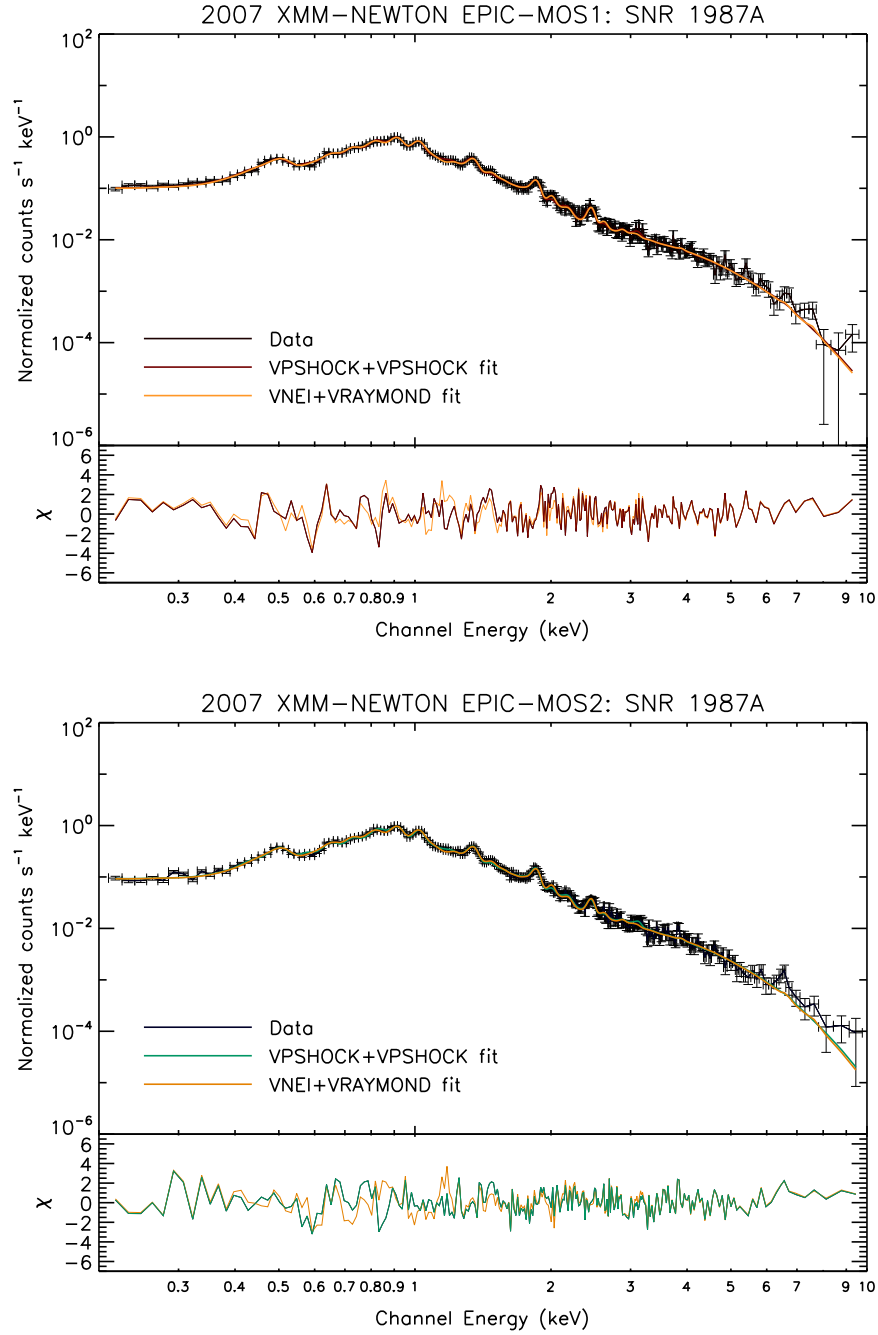


FIG. 4.— *XMM EPIC-MOS1* (top) and *EPIC-MOS2* (bottom) data, fitted by the VPSHOCK+VPSHOCK model. For the VPSHOCK+VPSHOCK model, the reduced chi-square values are $\chi_r^2 = 1.53$ (*MOS1*) and 1.40 (*MOS2*). For the VNEI+VRAYMOND model, the reduced chi-square values are $\chi_r^2 = 1.45$ (*MOS1*) and 1.46 (*MOS2*).

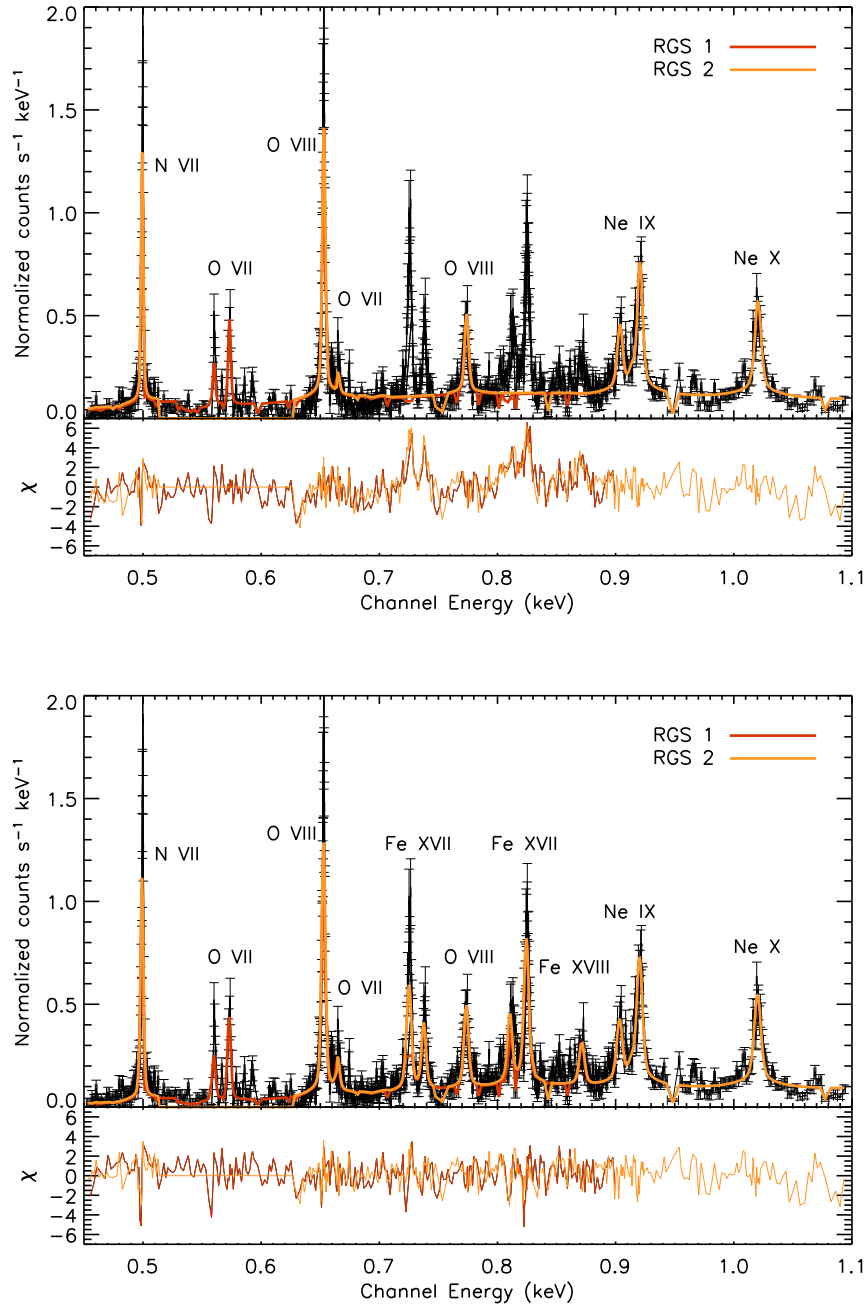


FIG. 5.— *XMM RGS* data considering 11 (top; $\chi_r^2 = 3.37$ for $N_{\text{dof}} = 652$) and 17 (bottom; $\chi_r^2 = 1.92$ for $N_{\text{dof}} = 645$) Gaussian fits to the lines, respectively (see text).

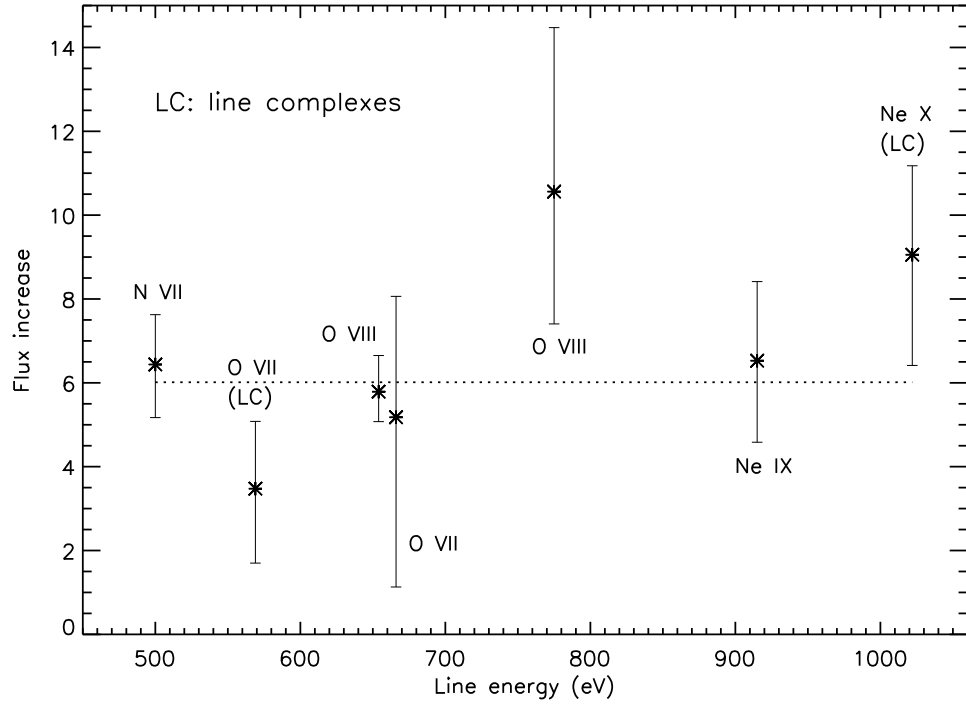


FIG. 6.— Flux increase in emission lines from *XMM RGS* data between 2003 May (Haberl et al. 2006) and this study (2007 Jan). The line complexes (denoted “LC”) represent the summed fluxes from three lines. See Table 5 and the text for details of the lines. The horizontal, dotted line shows a fit for the average increase in the line fluxes: 6.0 ± 0.6 ($\chi_r^2 = 0.98$).

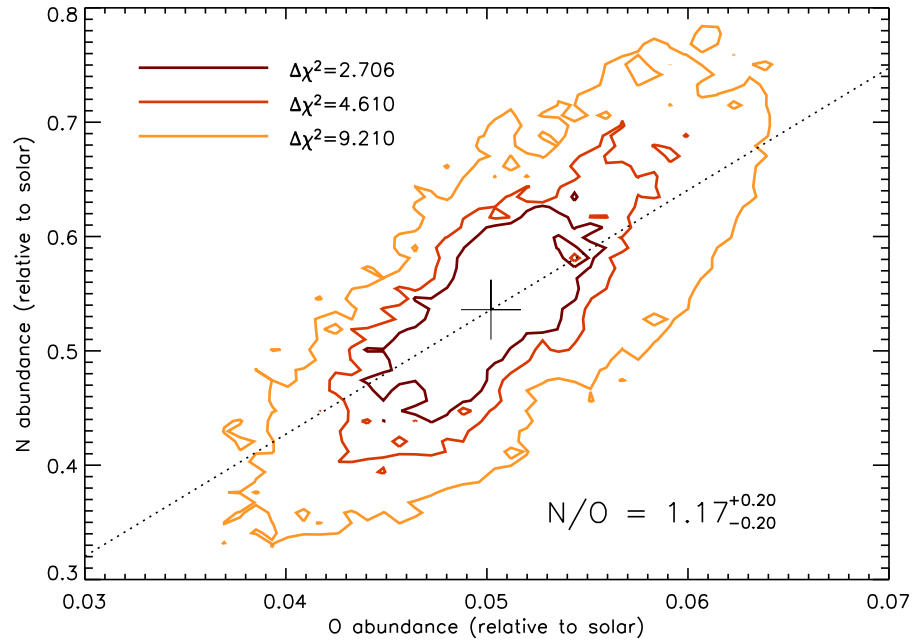


FIG. 7.— Contour map of N and O for various $\Delta\chi^2$ values from the best fit point, marked by the large cross. Values of N and O residing along the dotted line have the same N/O value as that for the best fit point.

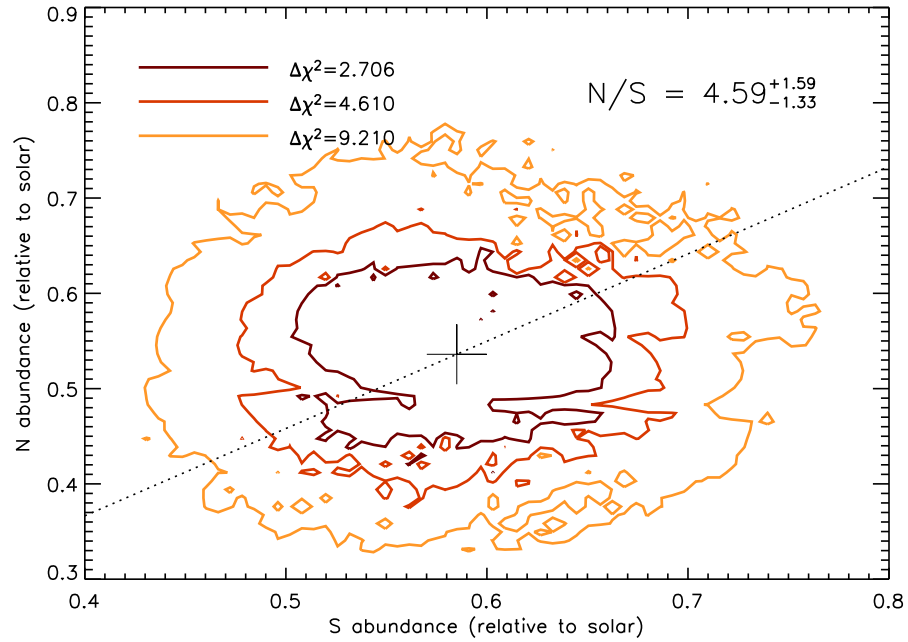


FIG. 8.— Same as Fig. 7, but for N/S.

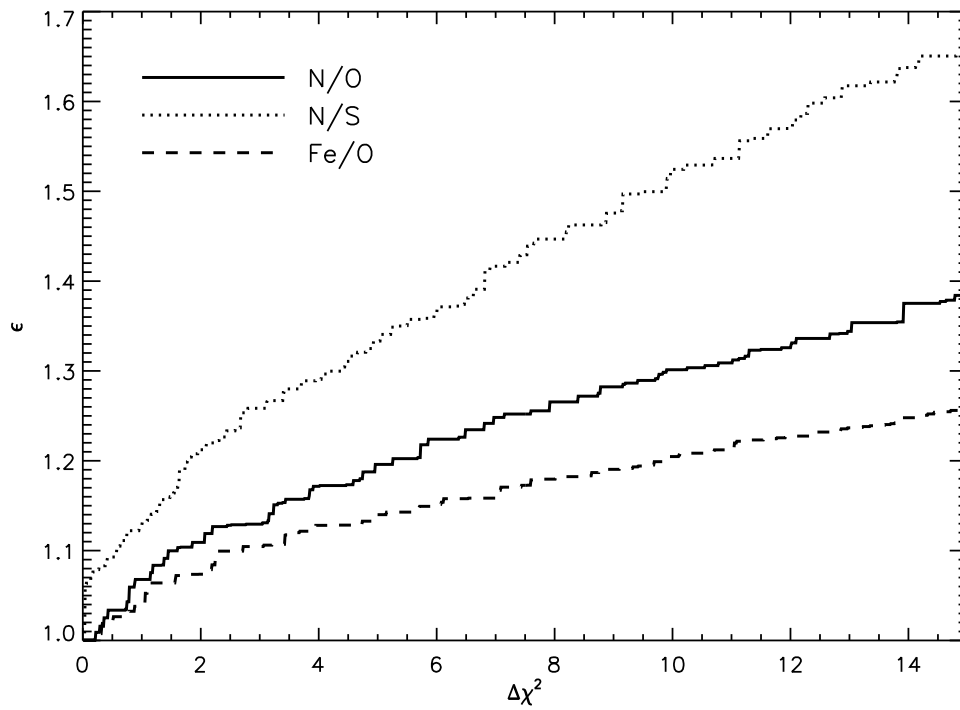


FIG. 9.— Mean error sustained by various abundance ratios as one moves $\Delta\chi^2$ away from the best fit point in the respective χ^2 maps.

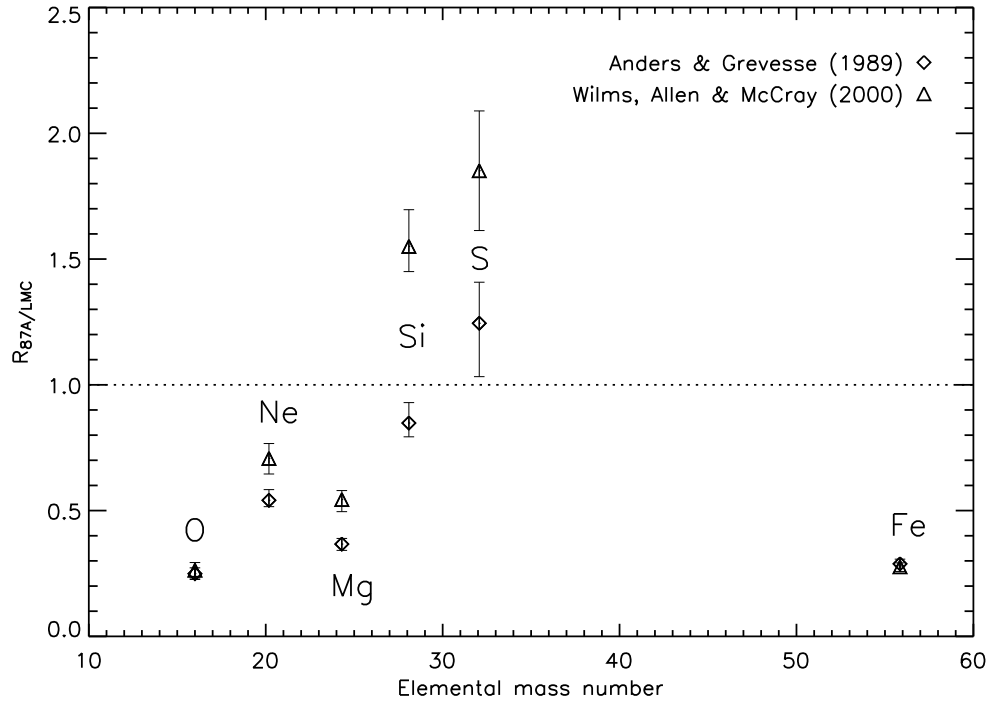


FIG. 10.— Abundance ratios of elements found by our study of SNR 1987A to the LMC quantities derived by Hughes, Hayashi & Koyama (1998). In our XSPEC analysis, we examine abundances obtained using the tables of Anders & Grevesse (1989) and Wilms, Allen & McCray (2000).